

This is a postprint version of the following published document:

Esposito, B.; Boncagni, L.; Buratti, P.; Carnevale, D.; Causa, F.; Gospodarczyk, M.; Martín-Solís, J.R.; Popovic, Z.; Agostini, M.; Apruzzese, G.; et al. (2017). Runaway electron generation and control. *Plasma Physics and Controlled Fusion*, 59(1), 014044, [12] p.

DOI: <https://doi.org/10.1088/0741-3335/59/1/014044>

© 2017 IOP Publishing Ltd.

# Runaway electron generation and control

B Esposito<sup>1</sup>, L Boncagni<sup>1</sup>, P Buratti<sup>1</sup>, D Carnevale<sup>2</sup>, F Causa<sup>1</sup>,  
M Gospodarczyk<sup>2</sup>, JR Martin-Solis<sup>3</sup>, Z Popovic<sup>3</sup>, M Agostini<sup>4</sup>,  
G Apruzzese<sup>1</sup>, W Bin<sup>5</sup>, C Cianfarani<sup>1</sup>, R De Angelis<sup>1</sup>, G Granucci<sup>5</sup>,  
A Grosso<sup>1</sup>, G Maddaluno<sup>1</sup>, D Marocco<sup>1</sup>, V Piergotti<sup>1</sup>, A Pensa<sup>1</sup>, S Podda<sup>1</sup>,  
G Pucella<sup>1</sup>, G Ramogida<sup>1</sup>, G Rocchi<sup>1</sup>, M Riva<sup>1</sup>, A Sibio<sup>1</sup>, C Sozzi<sup>5</sup>, B Tilia<sup>1</sup>,  
O Tudisco<sup>1</sup>, M Valisa<sup>4</sup> and FTU Team<sup>1</sup>

<sup>1</sup> Dipartimento FSN, ENEA, C. R. Frascati, via E. Fermi 45, 00044 Frascati (Roma), Italy

<sup>2</sup> Dip. di Ing. Civile ed Informatica DICII, Università di Roma, Tor Vergata, Roma, Italy

<sup>3</sup> Universidad Carlos III de Madrid, Avda. Universidad 30, Leganes, 28911-Madrid, Spain

<sup>4</sup> Consorzio RFX, Padova, Italy

<sup>5</sup> IFP-CNR, Via R. Cozzi 53, 20125 Milano, Italy

E-mail: [Basilio.Esposito@enea.it](mailto:Basilio.Esposito@enea.it)

## Abstract

We present an overview of FTU experiments on runaway electron (RE) generation and control carried out through a comprehensive set of real-time (RT) diagnostics/control systems and newly installed RE diagnostics. An RE imaging spectrometer system detects visible and infrared synchrotron radiation. A Cherenkov probe measures RE escaping the plasma. A gamma camera provides hard x-ray radial profiles from RE bremsstrahlung interactions in the plasma. Experiments on the onset and suppression of RE show that the threshold electric field for RE generation is larger than that expected according to a purely collisional theory, but consistent with an increase due to synchrotron radiation losses. This might imply a lower density to be targeted with massive gas injection for RE suppression in ITER. Experiments on active control of disruption-generated RE have been performed through feedback on poloidal coils by implementing an RT boundary-reconstruction algorithm evaluated on magnetic moments. The results indicate that the slow plasma current ramp-down and the simultaneous reduction of the reference plasma external radius are beneficial in dissipating the RE beam energy and population, leading to reduced RE interactions with plasma facing components. RE active control is therefore suggested as a possible alternative or complementary technique to massive gas injection.

Keywords: tokamak, runaway electrons, synchrotron radiation

## 1. Introduction

Two important ITER physics issues concerning the control and mitigation of runaway electrons (RE) are addressed in this paper: the measurement of the threshold electric field for RE *generation* and the *active control* of position and current ramp-down of disruption-generated RE. FTU experiments in this field have been strongly supported by the recent integration of diagnostic, hardware and software tools in the

real-time (RT) plasma control system. Several diagnostics used for RE measurements and control have been upgraded to RT operation and three new specific RE diagnostics have been installed: (a) a Cherenkov probe detecting escaping fast electrons to study the RE dynamics in presence of magnetic islands [1]; (b) an RE imaging system (REIS) to detect visible/infrared synchrotron radiation emitted by RE; (c) a hard x-ray (HXR) radial profile monitor measuring in-plasma bremsstrahlung from RE [2].

**Table 1.** Summary of diagnostics used for RE studies in FTU.

Diagnostic name	RE-related measured parameter	RE diagnostic capability	Time resolution (ms)	Energy range (keV)	Real-time (Y/N)	Main features	Reference
BF <sub>3</sub> chambers	Neutrons	Lost	5		N	Absolutely calibrated	[3]
<sup>235</sup> U fission chamber	Photoelectrons & photofissions	Lost	1		Y	Thick-target bremsstrahlung of $\gamma$ -rays $> \sim 7$ MeV	[4]
NaI scintillator	HXR	Lost/ confined	1		N	Pulse mode	[5]
	HXR spectra	Lost/ confined	100	$< 2 \times 10^3$	Y		[5]
NE213 scintillator	Neutrons, $\gamma$ -rays	Lost/ confined	0.05		N	Current mode, no $n/\gamma$ discrimination	[5]
Gamma camera	HXR radial profile	Confined	$\sim 1$	$> 100$	N	See text	[2]
Fast electron bremsstrahlung camera	HXR	Confined		20–200	N	Vertical and horizontal lines of sight	[6]
REIS	Synchrotron radiation spectra	Confined	$\sim 20$	—	N	See text	—
Cherenkov probe	Lost electrons	Lost	0.001	$> 58$	N	See text	[1]
CO <sub>2</sub> scanning interferometer	Electron density radial profile	Confined	0.0625	—	Y	Vertical chords at $R = (0.8965 - 1.2297)$ m MARTe RT implementation	[6, 7] [8]
MHD sensors	MHD modes	—	0.002	—	Y	Poloidal field pick-up Mirnov coils	[6]

## 2. Runaway electron diagnostics

A brief description of the diagnostic systems available for RE studies in FTU ( $R_0 = 0.935$  m,  $a = 0.3$  m) is given in table 1 above. More details can be found in the overview of the FTU diagnostics [6]. RE in flight in the plasma (confined) are detected by measuring SXR radiation, HXR bremsstrahlung, and infrared/visible synchrotron radiation, while RE that have escaped the plasma (lost) are measured by direct fast electron loss and gamma rays from thick target bremsstrahlung on plasma facing components (together with the corresponding neutrons produced in photonuclear reactions ( $\gamma, n$ )). Two of the three new FTU RE diagnostics are dedicated to the study of confined RE (*gamma camera* and *runaway electron imaging and spectrometry (REIS) system*), while the third investigates lost RE (*Cherenkov probe*). The *gamma camera* is a former neutron camera [9] optimized for RE studies through a digital upgrade (14-bit, 400 MSamples  $s^{-1}$ ) of its acquisition system [10]. Six collimated lines of sight (LOS) view the plasma from a lower vertical port; each LOS is equipped with a NE213 detector coupled to a PMT and an embedded <sup>22</sup>Na source for calibration purposes. The detectors are capable of  $n/\gamma$  discrimination, operated in count mode and sensitive to HXR with energy  $> 100$  keV. The gamma camera provides radially resolved measurements of HXR emitted perpendicularly to the magnetic field and produced by RE through bremsstrahlung in the plasma. The *REIS system* is a wide-angle optical diagnostic collecting the RE synchrotron radiation from two plasma cross sections (corresponding to the RE backward and forward views) and transmitting it to visible/infrared spectrometers through an incoherent bundle of fibres (figure 1); the spectral range spans from 300 to 2100 nm. The *Cherenkov probe* consists

of a single-crystal diamond detector mounted on a titanium zirconium molybdenum (TZM) head inserted into the FTU vessel [1]. The detector is coated with a 100/200/1000 nm Ti/Pt/Au interlayer filtering out visible light, particularly the plasma D $\alpha$  line. Electrons impinging on the probe emit Cherenkov radiation in diamond if  $v > c/n_d$  ( $v$  = electron speed,  $c$  = speed of light,  $n_d$  = refractive index of diamond), a condition corresponding to 58 keV electron energy threshold. The Cherenkov radiation is routed, through a visible/ultraviolet optical fibre, to a PMT operating in the 160–650 nm spectral range.

## 3. Runaway electron dynamics

The FTU RE diagnostics provide information on the various features of the RE dynamics (*spatial localization, energy and losses*). Radial profiles of HXR indicate that, in general, RE are initially produced in the centre of the plasma (see also [2]). Figure 2 provides an example: in discharge #39469 the appearance of RE is characterized by a peaked profile of the HXR line-integrals ( $t \sim 0.65$  s) (right); subsequently, as RE gain energy, as also shown by the rise of the photoneutron emission starting at  $t \sim 0.85$  s (left), the HXR emission peaks off-axis as a result of the RE radial losses and outward orbit drift. Past FTU measurements (HXR spectra from the NaI scintillator) have shown RE energies up to  $\sim 20$  MeV [5]. Novel measurements from the REIS diagnostic indicate even higher energies, in excess of 30 MeV. Consider discharge #39516 in which RE form already at  $\sim 0.05$  s, as shown (figure 3(left)) by the offset between the NE213 and BF<sub>3</sub> time traces (top) and the calculated Dreicer RE birth rate (secondary RE generation can be neglected in FTU) (middle).

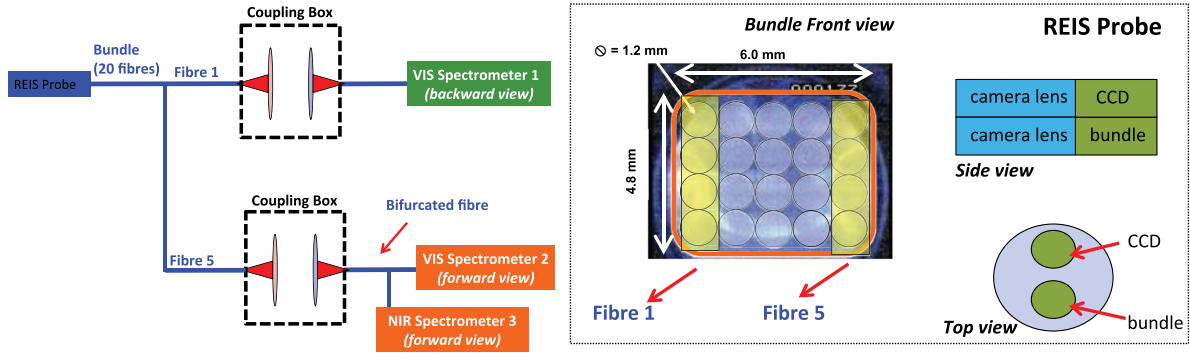


**Figure 1.** Layout of the runaway electron imaging and spectrometry (REIS) system. The REIS probe is composed by a wide-angle lens coupled to a CCD camera for the recording of video images (see figure 4) and a wide-angle lens coupled, through an incoherent bundle of fibres, to visible (VIS) and near-infrared (NIR) spectrometers for the acquisition of synchrotron spectra.

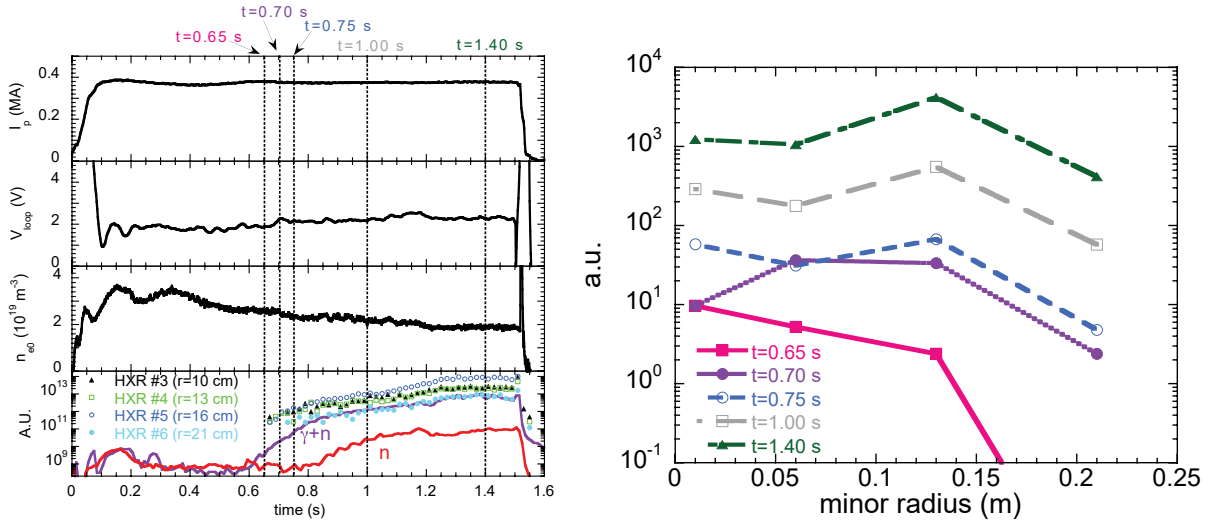


**Figure 2.** Discharge 39469 ( $B_t = 4.1$  T). (a) Time traces of plasma current ( $I_p$ ), loop voltage ( $V_{loop}$ ), line-averaged electron density ( $n_e$ ), line integrated HXR from gamma camera, HXR from NE213 scintillator and neutrons from BF<sub>3</sub>. (b) Radial profiles of line-integrated HXR emission from RE.

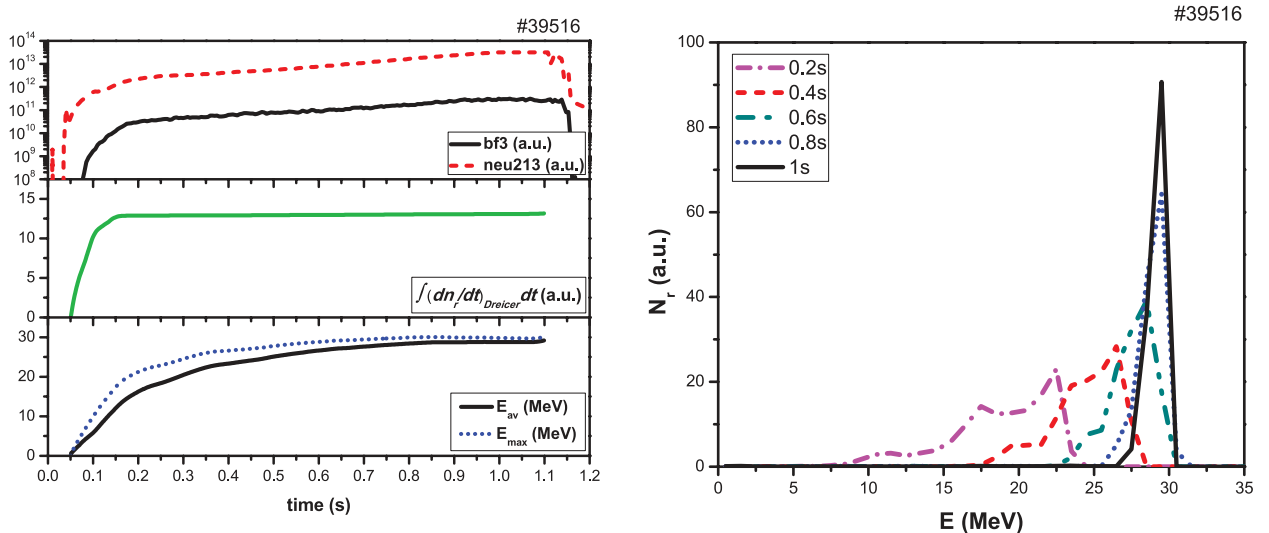


**Figure 3.** Discharge #39516 ( $B_t = 3.7$  T). (left) Generation of RE in a low density discharge: time traces of BF<sub>3</sub> and NE213 signals (top), calculated Dreicer birth rate (middle) and calculated average and maximum RE energy (bottom). (right) Calculated RE energy distributions.

For this discharge, figure 4 shows images of the RE beam from the visible camera correlated with the measured synchrotron radiation intensity at several wavelengths (right top) and the measured synchrotron radiation visible spectra (right bottom). The spectra are fitted (black solid lines) using formula (1) from [11] for a monoenergetic distribution.

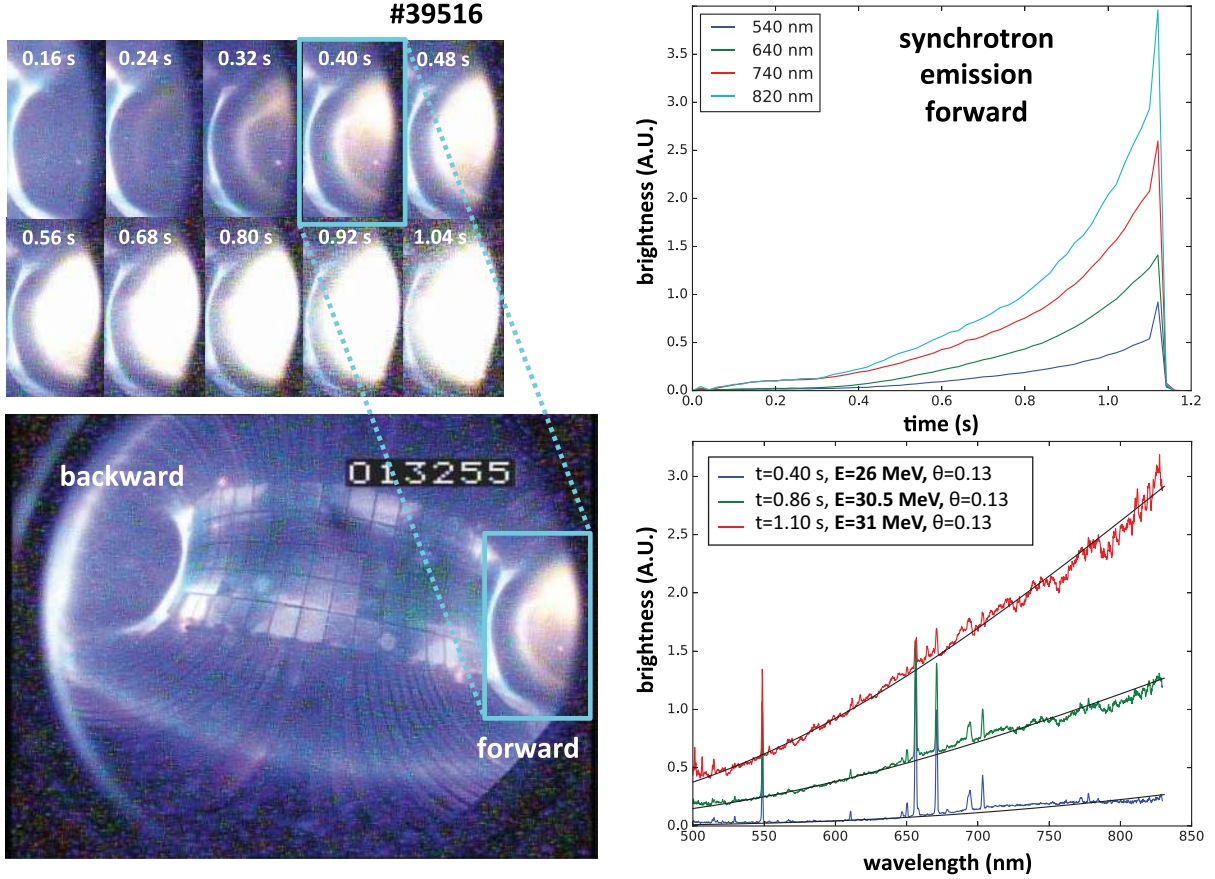


**Figure 4.** Discharge #39516 ( $B_t = 3.7$  T): Visible camera images of the RE beam (left): the bottom image (corresponding to frame 013255,  $t = 0.4$  s, of discharge #39516) shows both RE backward and forward views, while the top image is a time sequence of just the forward view for the same discharge. Note the temporal correlation of the visible images with the measured synchrotron radiation intensity at several wavelengths (right top) and synchrotron radiation visible spectra (right bottom): the spectra are fitted (solid lines) assuming monoenergetic distributions (energy and pitch angle values in the insert).

The measured energy and pitch angle values (see insert in figure 4(right bottom)) are in agreement with the predictions of simulations based on a test particle model of the RE dynamics [12] (figure 3(right)). The calculated RE energy distribution (figure 4(right)) gradually becomes monoenergetic with a maximum energy of  $\sim 30$  MeV (figure 4(left bottom)). Loss of RE from the plasma, often in correspondence with MHD events, is directly measured by the Cherenkov probe. An example is shown in figure 5 where phase-relations between Cherenkov, ECE and neutron (NE213 and BF<sub>3</sub>) signals show that the modulation of the Cherenkov signal associated with local RE losses is due to the magnetic island rotation [1]: most of RE are lost during the modulation phase, while some survive during the last part of the discharge (degraded confinement,  $t > 1$  s) and are lost at the disruption (HXR and photoneutron peaks).

#### 4. Runaway electron generation

RE represent a major threat in the operation of tokamaks, especially when generated in a disruption, and the understanding of the conditions that lead to their generation are important in the design of systems (such as massive gas injection (MGI)) dedicated to their suppression.

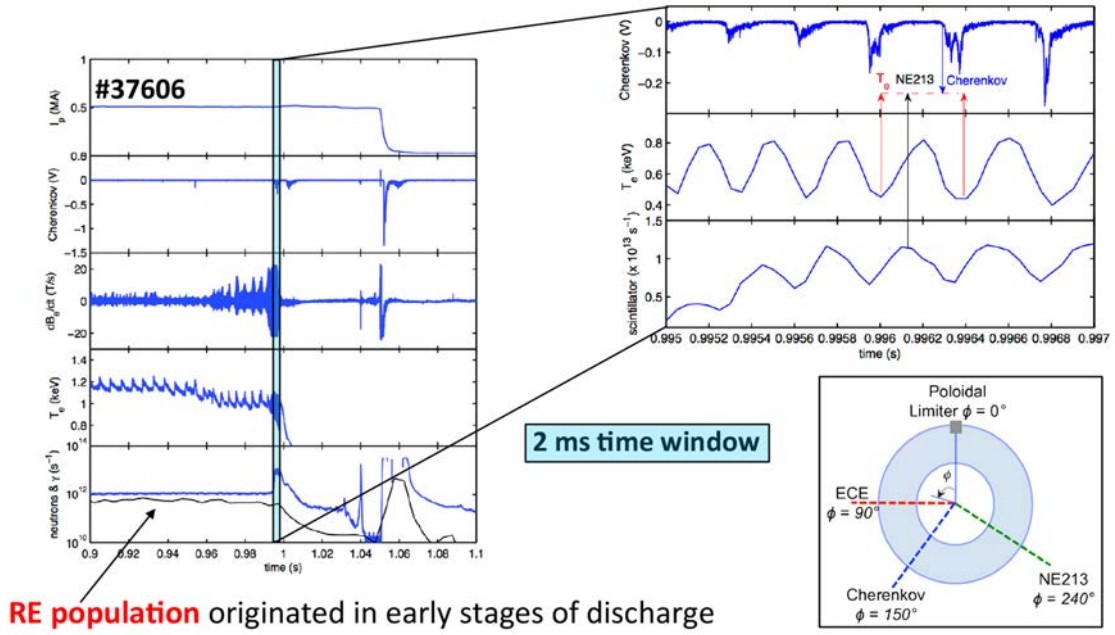
The relativistic collisional theory of RE generation [13] predicts that no REs can be generated below a critical electric field ( $E_R$ ) determined from the balance between electric field acceleration and collisional damping:

$$E_R = \frac{n_e e^3 \ln \Lambda}{4\pi \epsilon_0^2 m_e c^2}. \quad (1)$$

Hence, the necessary condition for RE avalanche growth is that the acceleration due to the toroidal electric field has to be higher than the collisional drag on the background particles,  $E > E_R$ .  $E_R$  scales linearly with the electron density  $n_e$ . The method adopted by the disruption mitigation system being designed for ITER to suppress RE avalanche growth is to raise  $n_e$  sufficiently high: however, the large quantity of injected gas may be problematic for subsequent machine operation.

There are various indications that other RE loss mechanisms may exist in addition to collisional damping:

- (a) The electron synchrotron radiation losses (neglected in the theory above) have been found to play an important role in RE suppression experiments by means of electron-cyclotron-resonance heating during the flat-top phase of FTU discharges [14]. It has been observed that RE suppression occurs at electric fields substantially larger than those predicted by the relativistic collisional



**RE population** originated in early stages of discharge

**Figure 5.** Discharge #37606 ( $B_t = 5.3$  T): Correlation between Cherenkov probe, ECE and NE213 signals showing loss of RE during MHD activity. Loss of a pre-existing RE population occurs at the time of the MHD event shown by the shaded area; a residual RE population survives until the disruption.

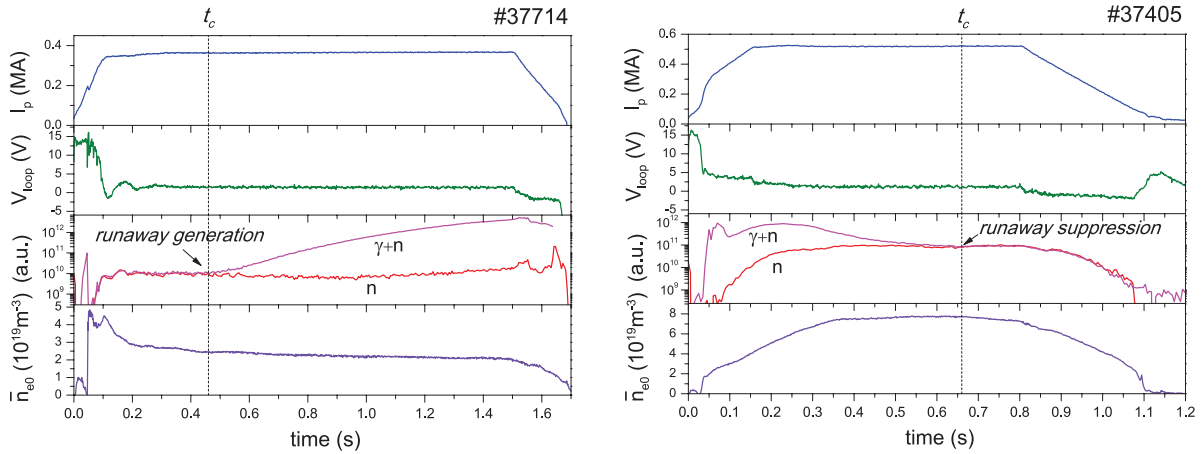


**Figure 6.** RE onset and suppression: time traces of  $I_p$ ,  $V_{loop}$ , NE213 ( $\gamma+n$ ) and  $BF_3$  ( $n$ ) signals and line-averaged central density.

theory of runaway generation. The experimental results are consistent with an increase of  $E_R$  due to the electron synchrotron radiation, which lead to a new electric field threshold  $E_R^{rad}$  [14]:

$$\frac{E_R^{rad}}{E_R} \cong 1 + C(Z_{eff})F_{gy}^\alpha \quad (2)$$

where

$$\alpha = 0.45 \pm 0.03; \quad F_{gy} \equiv \frac{2\varepsilon_0 B_0^2}{3n_e \ln \Lambda m_e};$$

$$C(Z_{eff}) \cong 1.64 + 0.53Z_{eff} - 0.015Z_{eff}^2. \quad (3)$$

(b) Data from the ITPA joint experiment to study RE generation and suppression in several tokamaks [15] show that the measured threshold electric field for RE generation

( $E_{thr}$ ) is 3–5 times higher than  $E_R$ , which, in turn, means that RE should be mitigated at densities lower than predicted.

The results of the systematic investigation of the conditions for RE generation in the plasma current ( $I_p$ ) flat-top phase of FTU deuterium ohmic discharges are reported here.  $E_{thr}$  has been evaluated in two different types of experiments: (1) *RE onset*; (2) *RE suppression*.

Figure 6 shows the time traces of  $I_p$ , loop voltage ( $V_{loop}$ ),  $BF_3$  chambers and NE213 scintillator signals and the central line-averaged electron density ( $\bar{n}_{e0}$ ) for an *RE onset* (left) and an *RE suppression* (right) experiment. The *RE onset* is obtained through a decreasing electron density ( $n_e$ ) in the  $I_p$  flat-top. The *RE suppression* is achieved by starting a discharge with low gas prefill, thus creating an RE population subsequently suppressed by a feedback-controlled phase of

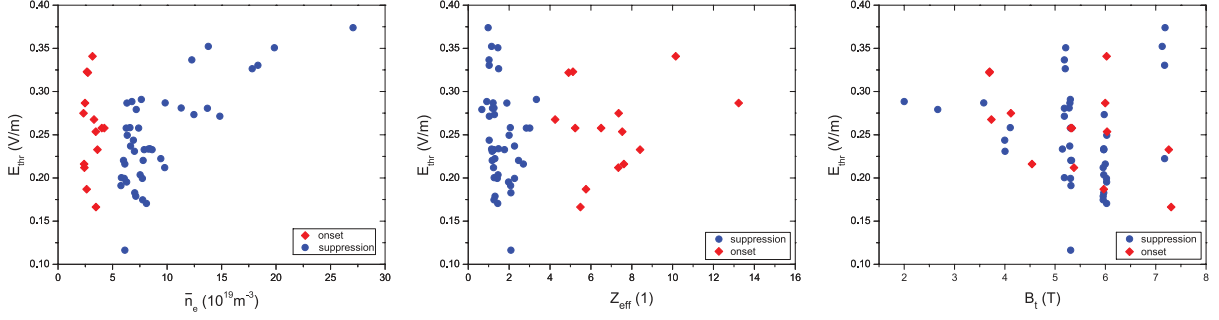


**Figure 7.** RE onset/suppression experiments: range of variability of the parameters appearing in synchrotron radiation theory formulas (2) and (3).

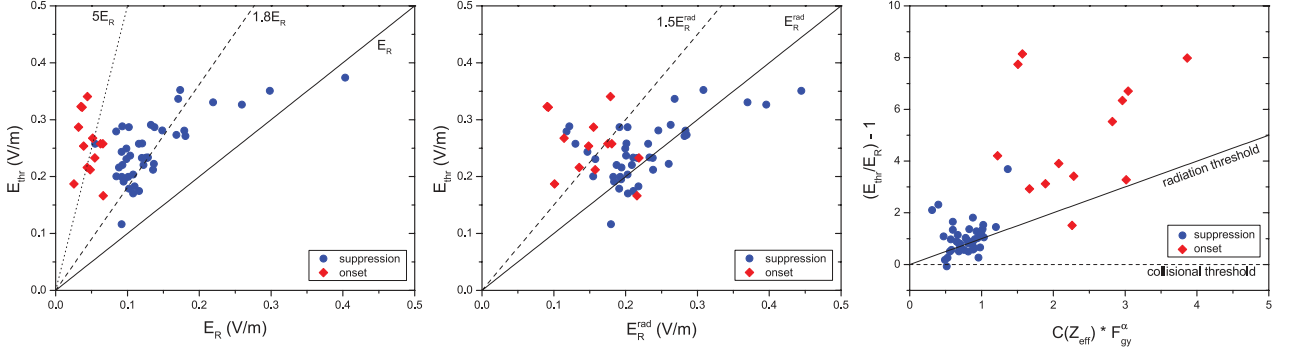


**Figure 8.** Comparison of measured  $E_{\text{thr}}$  with: (left) relativistic collisional radiation theory predictions ( $E_R$ ); (centre) relativistic collisional+synchrotron radiation theory predictions ( $E_R^{\text{rad}}$ ).

constant or increasing  $n_e$ . The time of *RE onset/suppression* is determined through the comparison of the time traces of the BF<sub>3</sub> and NE213 signals. In the *RE onset* experiments, during the pre-RE phase the NE213 signal overlaps with the BF<sub>3</sub> signal, while, as soon as the REs are generated, the two time traces diverge. On the other hand, in the *RE suppression* experiments, the NE213 signal is higher in the initial phase, indicating presence of RE, while later on, when *RE suppression* occurs, the two signals coincide. The time of the *RE onset/suppression* ( $t_c$  in the figures) is obtained by calculating the difference between the logarithms of the BF<sub>3</sub> and NE213 signals normalized to the NE213 signal and comparing it with the baseline value before the REs set in or after they disappear; the threshold field is then estimated as  $E_{\text{thr}} \sim \frac{V_{\text{loop}}(t_c)}{2\pi R_0}$ . Note that there is an instrumental limit for the minimum amount of RE that can be detected and this depends on the detector sensitivity: therefore, for example, some RE may be already present in the plasma while the BF<sub>3</sub> and NE213 signals still coincide.

The space of the variables of the synchrotron radiation theory formulas (2) and (3) (namely  $n_e$ , toroidal magnetic field ( $B_t$ ) and effective charge ( $Z_{\text{eff}}$ )) has been widely scanned in the experiments as shown by the three plots of figure 7, which show the range of measured  $E_{\text{thr}}$  values as a function of  $\bar{n}_{e0}$ ,  $B_t$  and  $Z_{\text{eff}}$  respectively. Each point corresponds to a different discharge. The database spans a wide range of plasma parameters:  $\bar{n}_{e0} = 2.3\text{--}27 \times 10^{19} \text{ m}^{-3}$ ,  $B_t = 2\text{--}7.2 \text{ T}$ ,  $Z_{\text{eff}} = 1.5\text{--}13$  and  $I_p = 0.35\text{--}0.9 \text{ MA}$ .

The measured  $E_{\text{thr}}$  values have been compared with the predicted  $E_R$  and  $E_R^{\text{rad}}$  (evaluated using the local central electron

density  $n_{e0}$ , instead of the line-averaged central density  $\bar{n}_{e0}$ , as it provides a better match with the experimental data). The plots of figures 8(left) and (center) indicate that the measured  $E_{\text{thr}}$  is  $\sim 2\text{--}5$  times larger than the threshold electric field,  $E_R$ , predicted by the classical collisional theory [13] while it is consistent with the new threshold calculated including synchrotron radiation losses [14]. In addition, the dependence of the new threshold on the plasma parameters ( $B_t$ ,  $Z_{\text{eff}}$  and  $n_e$ ) predicted by the synchrotron radiation theory (relations (2) and (3)) reasonably agrees with  $E_{\text{thr}}$ , as illustrated in figure 8(right). The differences observed in figure 8 between  $E_{\text{thr}}$  for the RE onset and suppression discharges are associated to the methodology used for determining  $E_{\text{thr}}$  in these experiments. During RE onset discharges, due to the limited sensitivity of the detectors, as explained above, some RE may already exist before the BF<sub>3</sub> and the NE213 time traces deviate from each other, so that the critical density is underestimated and, hence, the measured  $E_{\text{thr}}$  at given density is larger than the actual critical field. For the RE suppression experiments, the critical density is reached before the BF<sub>3</sub> and NE213 are observed to overlap (some time is required to suppress the REs once the critical conditions are reached). Therefore, the critical density inferred when the two signals overlap is larger than the real one and the measured  $E_{\text{thr}}$  at the given density will be lower than the actual critical field. Hence, the use of the RE onset and suppression experiments provide upper and lower bounds, respectively, for the critical field. Moreover, the error bars in the suppression experiments are likely to be larger than in the case of onset experiments and this may explain the larger scatter in suppression points data as found, for example, in figure 8(right).

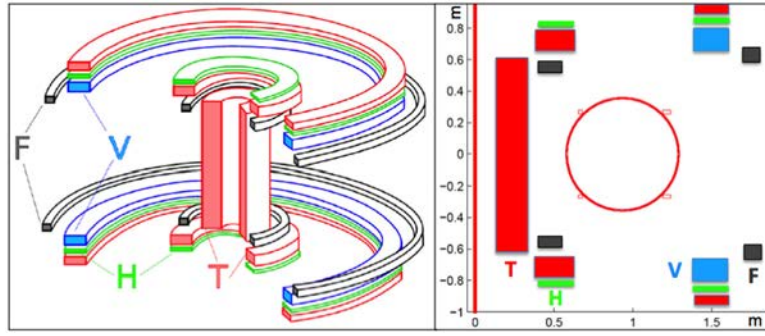


**Figure 9.** Active FTU coils. T controls the plasma current, V and F the plasma column radial movements and elongation, H the plasma column vertical position.

## 5. Runaway electron control

A crucial challenge towards a safe and efficient operation of ITER consists of the reduction of the dangerous effects of RE during disruptions [16]. RE are considered to be potentially intolerable for ITER when exhibiting currents larger than 2 MA. The main strategy to address this problem is RE suppression by means of MGI of High-Z noble gas before the thermal quench (TQ), which has the additional advantage of reducing the localized heat load. However, MGI leads to long recovery time, requires effective disruption predictors, and may lead to hot tail RE generation [17] or high mechanical loads if the current quench (CQ) does not occur in a suitable time interval [16, 18, 19]. In any circumstance in which such a suppression strategy may not be effective, for instance due to a delayed detection of the disruption and/or to a failure of the gas valves or of disruption avoidance techniques (e.g. using ECRH [20]) alternative RE mitigation strategies may be pursued, such as *resonant magnetic perturbations* to suppress RE [21–23] (however requiring specific active coils that are not available in FTU) and *RE active control* to dissipate the RE beam energy and population [24–26].

We present here FTU results on *RE active control*, i.e. stabilization of the disruption-generated RE beam (by minimizing its interaction with the PFCs). The RE energy dissipation is obtained by reducing the RE beam current via the central solenoid (inductive effects). In particular, the focus here is on those RE that survive the CQ. When the RE beam position is stabilized, further techniques, not studied in the present paper, such as high-Z gas injection to increase RE beam radiative losses could be exploited.

In the last few years, experiments on *RE active control* have been carried out in DIII-D [24], Tore Supra, FTU, JET, and initial studies have also been carried out at COMPASS [27]. In Tore Supra attempts at RE thermalization via MGI (He) have been investigated [28]. In DIII-D disruptions have been induced by injecting either Argon pellets or MGI while the ohmic coil current feedback has been left active to maintain constant current levels or to follow the reference current ramp-down [24]. DIII-D also studied the current beam dissipation rate by means of MGI with a final termination at approximately 100 kA [29]. Similar results on MGI mitigation of RE have been obtained at JET [30]. The present work goes along similar lines, but the RE beam dissipation is obtained only by

inductive effects, i.e. via central solenoid as in [24], combined with a new dedicated tool in the FTU plasma control system (PCS). This scheme provides an RE beam current ramp-down and position control. The effectiveness of the novel approach is measured in terms of reduced interaction of RE with the PFC.

Two novel real-time (RT) algorithms (*PCS-Ref1* and *PCS-Ref2*) for position and  $I_p$  ramp-down control of disruption-generated RE have been developed, implemented within the framework of the FTU PCS and tested in dedicated FTU plasma discharges. The active coils used to control the position and the current of the plasma are shown in figure 9.

The FTU PCS, extensively described in [31], exploits the current flowing within the T coil, called the central solenoid, to impose  $I_p$  via inductive effect. The T coil current  $I_T$  is regulated via a feedback control scheme based on a proportional–integral–derivative (PID) regulator, which is driven by the  $I_p$  error plus a pre-programmed signal. The horizontal position of the plasma is controlled by means of an additional PID regulator that is fed with the horizontal position error. Such error is obtained by on-line processing of a series of pick-up coil signals to determine the plasma boundary (last closed magnetic surface) which is compared along the equatorial plane to the reference plasma internal  $R_{int}$  and external  $R_{ext}$  radii, (see [32–35] for further details). The current flowing in the F coil ( $I_F$ ), by geometrical construction, allows us also to modify the plasma elongation  $\varepsilon$ . The current in the V coil ( $I_V$ ), which produces a vertical field similar to F but with a slower rate of change, is modified by a specific controller (Current Allocator [36]) in order to change  $I_F$  at run-time and maintain the vertical field unchanged. In such a way, the plasma radial position is left unchanged and at the same time it is possible to steer the value of  $I_F$  away from saturation levels. The current redistribution (reallocation) between  $I_F$  and  $I_V$  is performed by the Current Allocator at a slower rate than the changes imposed on  $I_F$  by the PID regulator (PID-F) for plasma horizontal stabilization. The PCS safety rules impose that whenever the HXR signal takes values above a given safety threshold for more than 10 ms, indication that harmful RE are present, the discharge has to be shut-down. In the *Standard* shut-down control algorithm the  $I_p$  reference is exponentially decreased down to zero and the reference inner and outer plasma radii at the equatorial plane ( $R_{int}$  and  $R_{ext}$ ) are left unchanged.



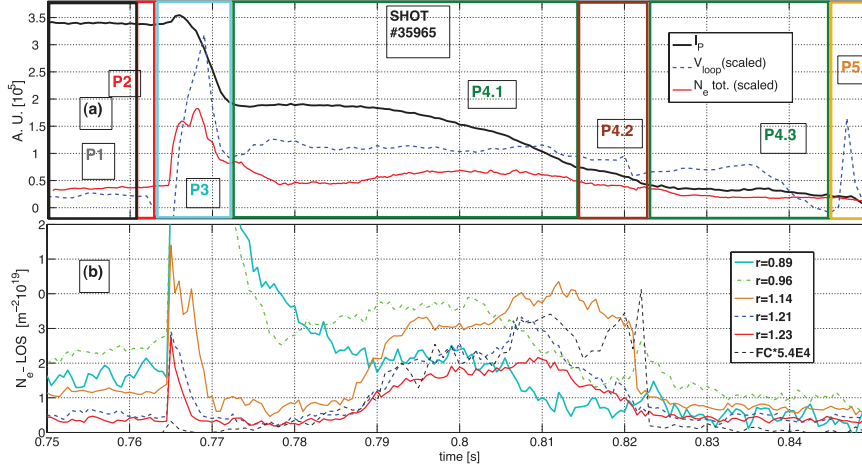


**Figure 10.** Discharge #35965: (a) plasma/RE current (black), total number of electrons computed from CO<sub>2</sub> interferometer (red solid), loop voltage (dashed blue). The different phases (P1 to P5) are highlighted. (b) CO<sub>2</sub> interferometer electron density line integrals compared with the FC signal (black dashed).

*PCS-Ref1* has been specifically designed for RE beam dissipation and comprises two different phases. In the first phase, specific algorithms described in [36] are employed to detect the CQ and the RE beam plateau by processing the  $I_p$  and the HXR signal. At the same time, the Current Allocator steers the values of  $I_F$  away from saturation limits, to ensure that a larger excursion is available for the control of the RE beam position. In the second phase, once the RE beam event has been detected (CQ or HXR level), the  $I_p$  reference is linearly ramped down in order to dissipate the RE beam energy by means of the central solenoid. A scan of the initial values and slope of the updated  $I_p$  reference for RE suppression (current ramp-down), that substitutes the standard  $I_p$  reference when the RE beam is detected, has been performed. At the same time, the reference external radius  $R_{ext}$  is reduced linearly with different slopes down to predefined constant values.  $R_{ext}$  is reduced in order to compensate for a large outward shift of the RE beam, hence to preserve the low field side vessel from RE beam impacts. The reduction of the  $R_{ext}$  reference can be considered the way of finding the RE beam radial position that provides minimal RE beam interaction with PFC: similar findings have been discussed in [24] and the RE beam position with minimal PFC interaction is called the ‘safe zone’. In all the experiments, the reference  $R_{int}$  is not changed since plasma operation is in (internal) limiter configuration. Nevertheless, the control system has the objective to maintain the plasma within the reference horizontal and vertical radii, avoiding plasma impact with the vessel (both sides).

*PCS-Ref2* has been designed with the same objective (RE beam control and energy suppression) as *PCS-Ref1*. The main difference consists in the fact that the updated reference  $R_{ext}$  is ramped down to a specific constant value (within the range 1.11–1.13 m) associated to a reduced level of the FC signal (as experienced in the experiments in which *PCS-Ref1* was active) plus a small time-varying term. This term (constrained to belong to the range  $(-0.04, 0.04)$  m), is computed in real-time by processing the measured  $R_{ext}$  and FC signals according to the extremum seeking technique (similar to a gradient algorithm discussed in [37, 38]) in order to minimize

the RT FC signal. Furthermore, the  $I_p$  ramp-down slope selected for *PCS-Ref2* is about three times slower compared to *PCS-Ref1*.

Due to the current amplifiers limitations, *PCS-Ref1* and *PCS-Ref2* are not expected to be effective in position and  $I_p$  current ramp-down control within 25–30ms of the CQ detection.

The two new RE active control algorithms have been tested in dedicated RE deuterium discharges. *PCS-Ref1* has been applied in an RE scenario in which a significant RE population is generated during the  $I_p$  ramp-up/flat top (360 kA, 6 T) by using a low gas prefill and a low density reference ( $1.5 \times 10^{19} \text{ m}^{-3}$ ), followed by an injection of neon gas to induce a disruption (*RE Scenario 1*). The sudden variation of the resistivity and the increased loop voltage at the disruption accelerate the pre-existing RE population and lead, in some cases, to the formation of an RE current plateau which is the target scenario of these experiments. Note that this scenario is not a method to create runaways but to turn an existing seed population of RE in a runaway plateau at the disruption. The discharge is run with an initial low gas prefill in such a way that early in the discharge ramp-up a runaway population is established. *PCS-Ref2* has been tested in an RE scenario differing from the first one by the use of an even lower gas prefill, which causes spontaneous disruption during the  $I_p$  ramp-up and, again, in some cases, an RE plateau (*RE Scenario 2*).

The characterization of the different phases of a disruption with the generation of an RE plateau is given in figure 10(a) for a typical discharge of *RE scenario 1*. After Ne gas injection, the plasma density slightly increases during the pre-disruptive phase P1. The TQ phase (P2), lasting a few milliseconds (1–2 ms), in which the plasma confinement is lost and the thermal energy is released to the vessel combined with the high electric field, produces a large increase of the electron density. The CQ phase (P3) follows: it is characterized by a sudden drop in  $I_p$  and a high self-induced parallel electric field ( $V_{loop}$ ) that further accelerates the pre-existing RE and possibly increases their number. The RE plateau phase (P4) follows and can be, in turn, divided into three sub-phases: in

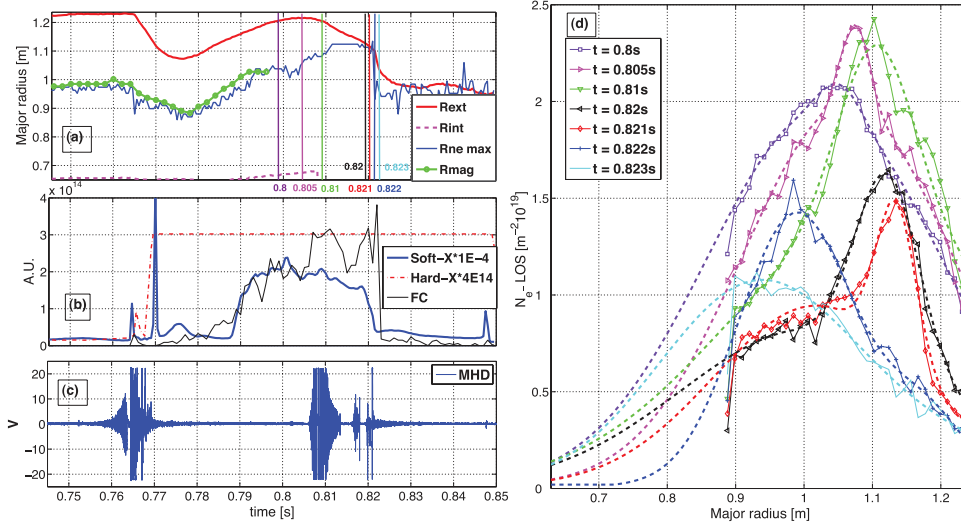


**Figure 11.** Discharge #35965 (a)  $R_{\text{ext}}$  (red solid),  $R_{\text{int}}$  (pink dashed),  $R_{\text{ne max}}$  (black),  $R_{\text{mag}}$  (green); (b) signals of SXR central line of sight (blue), HXR monitor (red), FC (black); (c) Mirnov coils; (d) radial profiles of electron density line integrals (solid = raw data, dashed = fitted data).

phase P4.1 the RE beam current exponentially replaces a large fraction of the ohmic  $I_p$  current (see [29], this process starts with the onset of the CQ); subsequently, part of such current can be lost due to instabilities (P4.2), while the rest of the beam can survive (further plateau in phase P4.3) before the final loss phase (P5).

Figure 10(b) shows the time traces of some of the  $\text{CO}_2$  interferometer electron density line integrals and the radial profiles of these integrals at different times are shown in figure 10(d). Note that the line integrals are available only in the range from 0.8965 m to 1.2297 m. The radial profiles of the line integrals have been fitted with Gaussian functions (least square minimization) in order to compute, by integration over the major radius  $R$  and toroidal angle, the total number of electrons ( $N_e$ ) and the major radius corresponding to the density peak ( $R_{\text{ne max}}$ ), as shown in figure 11(a): this panel also shows the radius of the magnetic axis as reconstructed by the ODIN equilibrium code ( $R_{\text{mag}}$ ), and the experimental inner and outer plasma radii at the equatorial plane from magnetic measurements ( $R_{\text{int}}$  and  $R_{\text{ext}}$ ). Finally, panels (b) and (c) show the signals from, respectively, the x-ray monitors and MHD coils.

The time traces of some of the  $\text{CO}_2$  interferometer electron density line integrals in the time interval between the RE plateau onset ( $\sim 0.775\text{--}0.82\text{ s}$ ) show that the cold plasma column is moving towards the low-field side: correspondingly, the FC signal increases due to the increased RE loss onto the outer limiter (phase P4.1). A large outer shift and an extremely peaked profile of the cold plasma column can be seen at approximately 0.81 s. An outward shift of the RE beam orbits is indeed a well known feature of the RE beam [24]. The RE beam is therefore centred on the right of  $R_{\text{ne max}}$ , although it is not possible to determine its position exactly.

The *PCS-Ref1* and *PCS-Ref2* RE active control results in *RE Scenario 1* and *RE Scenario 2* are shown in figures 12 and 13 respectively. The  $I_p$  reference at flat-top is typically 360 kA (500 kA for discharges #20532, #23448, #18723). The control algorithms replace the  $I_p$  reference by a linear ramp-down

as shown by the dashed lines in panel (e). Panels (b) and (f) show the measured (solid) and reference (dashed)  $R_{\text{ext}}$ .  $R_{\text{ext}}$  is kept constant (1.23 m) in the *Standard* control algorithm, whereas in *PCS-Ref1/2* it is changed dynamically at run-time. Note that the control system, after the initial CQ phase, does not fully succeed to steer  $R_{\text{ext}}$  to the reference value. This lack of performance is due to the fact that  $I_p$  is simultaneously ramping down, inducing a bias in the radial plasma position error. In the future, a new radial controller with double integrator [39] will be used in order to get rid of such bias. The following other signals are shown:  $V_{\text{loop}}$  in panels (c) and (g), FC (solid) and HXR (dashed) in panels (d) and (h), NE213 scintillator in panels (i) and (l).

### 5.1. RE scenario 1/PCS-Ref1

The start of the  $I_p$  ramp-down has been varied in different pulses by modifying specific parameters of the CQ detector, whereas the ramp-down slopes have been set directly modifying the controller configuration file. The new  $I_p$  reference allows us to define an updated  $I_p$  error that is fed to the PID-T controller. The PID-T acts on a current amplifier in order to change the current flowing within the central solenoid  $I_T$ , thus obtaining an RE beam current suppression by induction. The new  $I_p$  reference ramp-down induces a lower  $V_{\text{loop}}$  than in the standard case (figures 12(c) and (g)), due to the action of the control system that modifies the rate of the current in the central solenoid coil, hence reducing the energy transferred by the central solenoid to the RE and, consequently, reducing also the RE radial outward shift. On the contrary, in the *Standard* control algorithm the effort of the PCS to recover the flat-top  $I_p$  value induces large voltages that increase the RE energy and also their outward shift. Simultaneously, the smaller new  $R_{\text{ext}}$  reference contributes to the reduction of the RE beam interaction with the low-field side wall. The improvement of *PCS-Ref1* discharges in terms of reduced FC signal is quite evident (note the different scales in the FC panels), especially

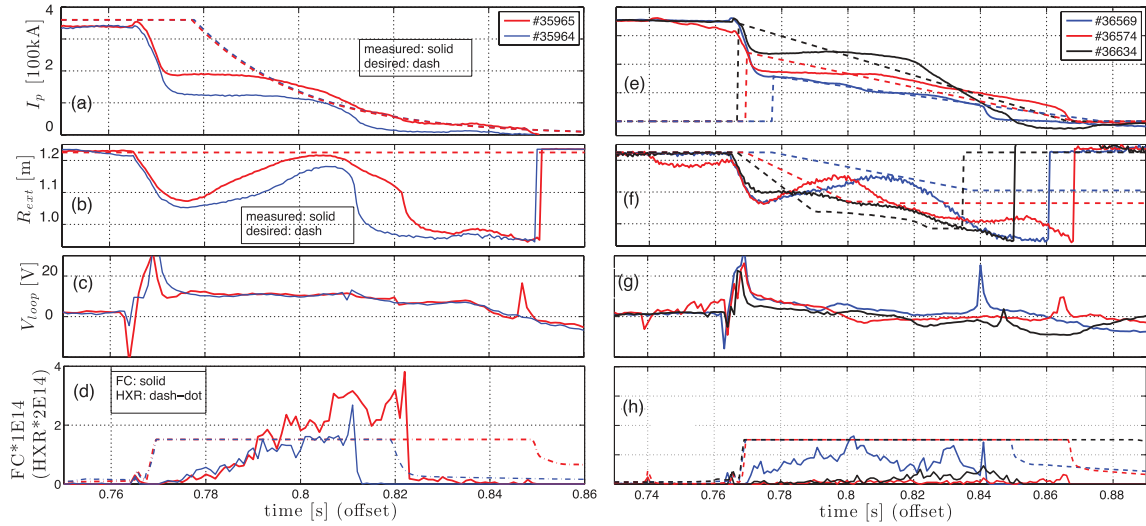


**Figure 12.** Scenario 1 (RE produced in a low gas prefill and a low density reference, followed by an injection of neon gas to induce a disruption): (left) no runaway control (*Standard algorithm*); (right) runaway active control (*PCS-Ref1 algorithm*).

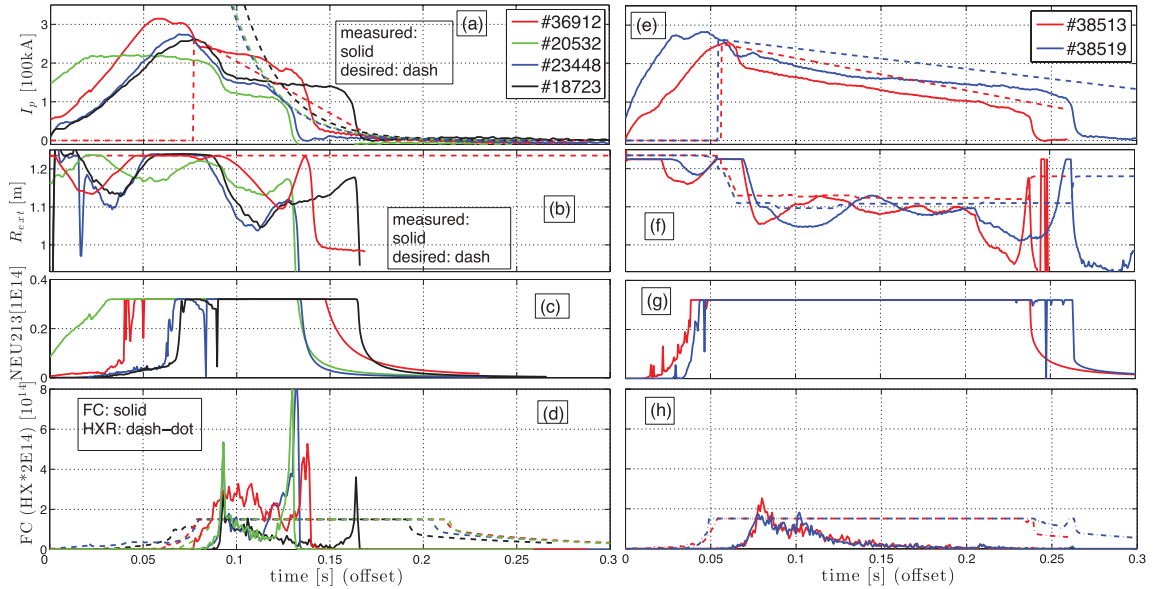


**Figure 13.** Scenario 2 (RE plateau in spontaneous disruption during the  $I_p$  ramp-up) (left) no runaway control (*Standard algorithm*); (right) runaway active control (*PCS-Ref2 algorithm*).

for discharges #36574 and #36634 where  $R_{ext}$  is reduced by more than 10% with respect to the standard value.

## 5.2. RE scenario 2/PCS-Ref2

The controller is not activated by the detection of the CQ or current plateau onset, as in *Scenario 1*, but when the HXR signal exceeds the safety threshold. Both hard x-ray monitors (NE213 and HXR) are saturated following the CQ throughout the  $I_p$  ramp-down indicating that energetic RE are present.  $R_{ext}$  is set to an initial value but, afterwards, is adjusted in RT: the RT FC signal is exploited to slightly modify  $R_{ext}$  and minimize the FC signal itself. Note the sudden ramp down of  $R_{ext}$  to 1.11 m and 1.13 m, respectively, in discharges #38519 and #38513 and the subsequent slight changes in time. The following improvements are observed when using *PCS-Ref2*:

- discharges with *RE active control* show a reduction of the FC signal down to zero during the slow  $I_p$  ramp-down and  $R_{ext}$  decrease, while those with no *RE active control* disrupt earlier and show a large FC final peak at the RE loss;
- despite the larger RE beam final current loss in *PCS-Ref2* with respect to *PCS-Ref1* the corresponding final FC peaks are noticeably smaller, almost negligible;
- the HXR signal drops below the saturation value before the final loss in #38519 unlike the other discharges: since the current drop at the final loss is about 100 kA, this may suggest that a considerable RE beam energy has been dissipated (electron thermalization) during the  $I_p$  ramp-down;
- the use of a  $R_{ext}$  RT reference constrained by the FC RT signals seems to improve the capability of the control to

maintain the RE beam for longer time intervals than in *PCS-Ref1* (up to 200 ms).

The *PCS-Ref1/2* results suggest the importance of reducing the external plasma radius reference to minimize the RE interactions with the vessel, confirming similar results discussed in [24].

## 6. Conclusions

The RE energy and pitch angle inferred from spectral synchrotron radiation measurements of the novel RE imaging and spectrometry (REIS) diagnostic installed in FTU are found to be consistent with the predictions of a test particle model of the RE dynamics. Energy values of over 30 MeV and pitch angles of the order of 0.1 rad have been measured. HXR profile measurements of RE bremsstrahlung interactions have shown that RE due to Dreicer generation appear in the plasma center and subsequently drift outwards. Details on the local RE losses linked to MHD activity are provided by a Cherenkov probe.

Dedicated experiments on RE onset and suppression in FTU provide, respectively, measurements of the upper and lower bounds of the threshold electric field for RE generation ( $E_{\text{thr}}$ ) and indicate that  $E_{\text{thr}}$  is larger by a factor  $\sim 2\text{--}5$  than expected according to the purely collisional theory; on the contrary,  $E_{\text{thr}}$  reasonably agrees with the new threshold calculated including synchrotron radiation losses. This confirms earlier results from FTU RE suppression experiments carried out in presence of electron-cyclotron heating [14]. Moreover, the theoretical dependence of the new threshold on the plasma parameters ( $B_v$ ,  $Z_{\text{eff}}$  and  $n_e$ ) is also matched reasonably well by the experimental data. These findings might imply a lower threshold density value to be achieved by means of massive gas injection for RE suppression in ITER. However, it is still an open question whether such results, that are obtained in the  $I_p$  flat-top of ohmic plasmas, can be confirmed for disruption-generated RE.

Two algorithms for the *active control* of disruption-generated RE have been implemented in FTU: they redefine in real-time the external plasma radius ( $R_{\text{ext}}$ ) and  $I_p$  ramp-down references, exploiting magnetic and gamma-ray signals. The  $I_p$  ramp-down is performed via the central solenoid and the current in the poloidal coils is changed to control the position of the RE beam as determined by the magnetic measurements. It has been shown that by means of a slow  $I_p$  ramp-down ( $\sim 1 \text{ MA s}^{-1}$  up to 200 ms) and of a reduction of  $R_{\text{ext}}$  (approximately 10% of the flat-top value), there are indications of RE beam energy suppression and reduced interactions with the vessel (especially in the low-field side), thus prompting *RE active control* as alternative/complementary technique to MGI. Further work is necessary to better refine the optimal  $R_{\text{ext}}$  reference during the RE beam  $I_p$  ramp-down, possibly defined as a function of  $I_p$  and RE beam energy. Moreover, the availability of real-time density profile from the scanning interferometer will allow improvement of the estimate of the runaway beam radial position and enable more robust runaway beam suppression strategies. Future plans also include a re-design of the PID-T and PID-F current and position controllers—based

on an RE beam dynamical model—to further improve their performances, specifically in the RE control phase.

## Acknowledgements

This work was carried out within the framework of the EURO-fusion Consortium and received funding from the Euratom research and training programme 2014–2018 under grant agreement No 633053 (Projects MST2-9 and MST2-15). The views and opinions expressed herein do not necessarily reflect those of the European Commission. Additional financial support was received from MINECO (Spain), Projects No. ENE2012-31753 and ENE2015-66444-R.

## References

- [1] Causa F *et al* 2015 Cherenkov emission provides detailed picture of non-thermal electron dynamics in the presence of magnetic islands *Nucl. Fusion* **55** 123021
- [2] Marocco D *et al* 2015 First results on runaway electron studies using the FTU neutron camera *Fusion Eng. Des.* **96–7** 852
- [3] Bertalot L *et al* 1992 Improved calibration of the neutron yield measurement system on the FTU tokamak *Rev. Sci. Instrum* **63** 4554
- [4] Martin-Solis J R *et al* 2014 Inter-machine comparison of the termination phase and energy conversion in tokamak disruptions with runaway current plateau formation and implications for ITER *Nucl. Fusion* **54** 083027
- [5] Esposito B *et al* 2003 Dynamics of high energy runaway electrons in the Frascati Tokamak Upgrade *Phys. Plasmas* **10** 2350
- [6] Tudisco O *et al* 2004 Chapter 8: The diagnostic systems in the FTU *Fusion Sci. Technol.* **45** 402
- [7] Canton A, Innocente P and Tudisco O 2006 Two-color medium-infrared scanning interferometer for the Frascati tokamak upgrade fusion test device *Appl. Opt.* **45** 9105
- [8] Boncagni L *et al* 2016 MARTE real-time acquisition system of a two-color interferometer for electron density measurements on FTU (Frascati tokamak upgrade) *Proc. 20th IEEE-NPSS Real-Time Conf.*
- [9] Batistoni P *et al* 1995 Design of the neutron multicollimator for Frascati tokamak upgrade *Rev. Sci. Instrum.* **66** 4949
- [10] Riva M 2013 Real time  $n/\gamma$  discrimination for the JET neutron profile monitor *Fusion Eng. Des.* **88** 1178
- [11] Stahl A *et al* 2013 Synchrotron radiation from a runaway electron distribution in tokamaks *Phys. Plasmas* **20** 093302
- [12] Popovic Z *et al* 2016 On the measurement of the threshold electric field for runaway electron generation in the Frascati Tokamak Upgrade *Phys. Plasmas* accepted for publication
- [13] Connor J W and Hastie R J 1975 Relativistic limitations on runaway electrons *Nucl. Fusion* **15** 415
- [14] Martin-Solis J R *et al* 2010 Experimental observation of increased threshold electric field for runaway generation due to synchrotron radiation losses in the FTU tokamak *Phys. Rev. Lett.* **105** 185002
- [15] Granetz R *et al* 2014 An ITPA joint experiment to study runaway electron generation and suppression *Phys. Plasmas* **21** 072506
- [16] Lehnen M *et al* 2015 Disruptions in ITER and strategies for their control and *J. Nucl. Mater.* **463** 39
- [17] Smith H M and Verwichte E 2008 Hot-tail runaway electron generation in tokamak disruptions *Phys. Plasmas* **15** 072502
- [18] Putvinski S 2010 Disruption mitigation in ITER *Proc. 23rd IAEA Fusion Conf.* vol 43 ITR/1–6

- [19] Hollmann E *et al* 2015 Status of research toward the ITER disruption mitigation system *Phys. Plasmas* **22** 021802
- [20] Esposito B *et al* 2009 Disruption control on FTU and ASDEX upgrade with ECRH *Nucl. Fusion* **49** 065014
- [21] Lehnen M *et al* 2008 Suppression of runaway electrons by resonant magnetic perturbations in TEXTOR disruptions *Phys. Rev. Lett.* **100** 255003
- [22] Papp G *et al* 2011 Runaway electron losses enhanced by resonant magnetic perturbations *Nucl. Fusion* **51** 043004
- [23] Matsuyama A, Yagi M and Kagei Y 2013 Stochastic transport of runaway electrons due to low-order perturbations in tokamak disruption *Proc. of the 12th Asia Pacific Physics Conf. (APPC12)* JPSCP.1.015037
- [24] Eidietis N W *et al* 2012 Control of post-disruption runaway electron beams in DIII-D *Phys. Plasmas* **19** 056109
- [25] Lukash V *et al* 2013 Study of ITER plasma position control during disruptions with formation of runaway electrons *Proc. 40th EPS Conf. Plasma Physics* P5.167
- [26] Snipes J A *et al* 2014 Physics of the conceptual design of the ITER plasma control system *Fusion Eng. Des.* **89** 507
- [27] Vlainic M *et al* 2015 Post-disruptive runaway electron beam in COMPASS tokamak *J. Plasma Phys.* **81**
- [28] Saint-Laurent F *et al* 2011 Control of runaway electron beam heat loads on torus supra *Proc. 38th EPS Conf. Plasma Physics* O3 118
- [29] Hollmann E M *et al* 2013 Control and dissipation of runaway electron beams created during rapid shutdown experiments in DIII-D *Nucl. Fusion* **53** 083004
- [30] Lehnen M *et al* 2011 Disruption mitigation by massive gas injection in JET *Nucl. Fusion* **51** 123010
- [31] Boncagni L *et al* 2014 An overview of the software architecture of the plasma position, current and density real-time controller of the FTU *Fusion Eng. Des.* **89** 204
- [32] Astolfi A *et al* 2014 Adaptive hybrid observer of the plasma horizontal position at FTU *22nd Mediterranean Conf. Control and Automation* p 1088
- [33] Ariola M and Pironti A 2008 *Magnetic Control of Tokamak Plasmas* (London: Springer)
- [34] Boncagni L *et al* 2011 First steps in the FTU migration towards a modular and distributed real-time control architecture based on MARTe *IEEE Trans. J. Nucl. Sci.* **58** 1778
- [35] Boncagni L *et al* 2012 MARTe at FTU: the new feedback control *Fusion Eng. Des.* **87** 1917
- [36] Boncagni L *et al* 2013 A first approach to runaway electron control in FTU *Fusion Eng. Des.* **8** 1109
- [37] Carnevale D *et al* 2009 A new extremum seeking technique and its application to maximize RF heating on FTU *Fusion Eng. Des.* **84** 554
- [38] Carnevale D *et al* 2008 Extremum seeking without external dithering and its application to plasma RF heating on FTU *47th IEEE Conf. Decision and Control (CDC)* p 3151
- [39] Boncagni L *et al* 2015 Performance-based controller switching: an application to plasma current control at FTU *54th IEEE Conf. Decision and Control (CDC)* p 2319